Precambrian Research 177 (2010) 241–252

Contents lists available at ScienceDirect

Precambrian Research

journal homepage: www.elsevier.com/locate/precamres

Carbon and sulfur isotope chemostratigraphy of the Neoproterozoic Quanji Group of the Chaidam Basin, NW China: Basin stratification in the aftermath of an Ediacaran glaciation postdating the Shuram event?

Bing Shen[a,b,*], Shuhai Xiao[a], Chuanming Zhou[c], Alan J. Kaufman[d], Xunlai Yuan[c]

[a] Department of Geosciences, Virginia Polytechnic Institute and State University, Blacksburg, VA 24061, USA
[b] Department of Earth Science, Rice University, Houston, TX 77005, USA
[c] State Key Laboratory of Paleobiology and Stratigraphy, Nanjing Institute of Geology and Paleontology, Chinese Academy of Sciences, Nanjing 210008, China
[d] Department of Geology, University of Maryland, College Park, MD 20742, USA

ARTICLE INFO

Article history:
Received 15 June 2009
Received in revised form
30 November 2009
Accepted 23 December 2009

Keywords:
Ediacaran
Glaciation
Carbon isotopes
Sulfur isotopes
Chaidam Basin
Quanji Group

ABSTRACT

The Neoproterozoic Quanji Group in the Chaidam Basin, northwest China, consists of, in ascending order, the Mahuanggou, Kubaimu, Shiyingliang, Hongzaoshan, Heitupo, Hongtiegou, and Zhoujieshan formations. It is a siliciclastic-dominated sequence with only two carbonate units, the ~300-m-thick Hongzaoshan dolostone and the ~4-m-thick Zhoujieshan cap dolostone, the latter of which lies above the Hongtiegou glacial diamictite. In this study, we analyzed the $\delta^{13}C$ and $\delta^{18}O$ of the Hongzaoshan dolostone and Zhoujieshan cap dolostone, and the $\delta^{34}S_{CAS}$, $\delta^{34}S_{py}$, and trace element compositions (Fe, Mn, Sr, and S) of the Zhoujieshan cap dolostone. $\delta^{13}C$ profile of the Hongzaoshan dolostone shows a shift from −5‰ to 0‰. This shift could be correlated with a similar shift in the Shuiquan Formation (<615 ± 6 Ma) in the Quruqtagh area of the Tarim Block (NW China), and may be equivalent to negative $\delta^{13}C$ excursions in the middle or uppermost Doushantuo Formation, the latter of which is widely believed to be correlative with the Shuram negative $\delta^{13}C$ excursion. This correlation, together with available paleontological evidence (fragments of *Redkinia* from the Heitupo Formation, a genus that also occurs in ~555 Ma successions in the East European Platform), suggests that the Hongtiegou diamictite may represent an Ediacaran glaciation postdating the Gaskiers glaciation or occurring near the Precambrian–Cambrian boundary. The Zhoujieshan cap dolostone is characterized by positive $\delta^{13}C$ values ranging from 0‰ to +1.7‰, in sharp contrast to cap carbonates overlying the Sturtian and Marinoan diamictites. $\delta^{34}S_{CAS}$ of the Zhoujieshan cap dolostone varies strongly between +13.9‰ and +24.1‰, probably due to relatively low-sulfate concentration in seawater. $\delta^{34}S_{py}$ values, however, show a steady increase from +12.9‰ to +26.4‰. Thus, $\delta^{34}S_{CAS}$ and $\delta^{34}S_{py}$ trends are decoupled in the Zhoujieshan cap dolostone, and the high $\delta^{34}S_{py}$ values in the upper part of the cap dolostone indicate inverse sulfur isotope fractionations ($\delta^{34}S_{CAS} < \delta^{34}S_{py}$). The decoupling of $\delta^{34}S_{CAS}$ and $\delta^{34}S_{py}$ suggests that CAS and pyrite were derived from different sulfur pools (a possible scenario if the post-glacial Oulongbluq basin was restricted and stratified) and/or that aerobic oxidation of sulfide was intense in the post-glacial Oulongbluq basin.

Published by Elsevier B.V.

1. Introduction

Available geochronological data require at least four Neoproterozoic glaciations (Xu et al., 2009). These are, in chronological order, the Kaigas (Frimmel et al., 1996), Sturtian (Allen et al., 2002; Fanning and Link, 2004; Kendall et al., 2006), Marinoan (Hoffmann et al., 2004; Zhou et al., 2004; Condon et al., 2005), and Ediacaran Gaskiers glaciation (Bowring et al., 2003). Of these, only the Marinoan glaciation and maybe the Sturtian glaciation are demonstrably global. There has been intensive discussion in the literature about the Sturtian and Marinoan glaciations, but Ediacaran glaciations are poorly documented, partly because of their limited geographic distributions. Unlike Marinoan-age glacial diamictites, which are typically overlain by a cap carbonate, cap carbonates associated with Ediacaran glacial diamictites are poorly developed. So far, only the Gaskiers diamictite in Newfoundland (Myrow and Kaufman, 1999), the Hankalchough diamictite in Quruqtagh of NW China (Xiao et al., 2004), the Baykonur diamictite in Kazakhstan and Kyrgyzstan (Chumakov, 2009), and the Egan in Western Australia (Corkeron, 2007) are known to be Ediacaran diamictites overlain by cap carbonates. The $\delta^{13}C$ values of these cap carbonates

* Corresponding author at: Department of Earth Science, Rice University, Ms126, 6100 Main St., Houston, TX 77005, USA. Tel.: +1 281 733 6317.
E-mail address: bing.shen@rice.edu (B. Shen).

0301-9268/$ – see front matter. Published by Elsevier B.V.
doi:10.1016/j.precamres.2009.12.006

are quite variable (Myrow and Kaufman, 1999; Xiao et al., 2004; Corkeron, 2007). Therefore, there is a great need to acquire more chemostratigraphic data in order to characterize and understand their chemostratigraphic variations. The Zhoujieshan cap dolostone that overlies the Ediacaran Hongtiegou diamictite of the Quanji Group in the Chaidam Basin, northwest China, offers such an opportunity. In this paper, we describe the lithostratigraphy and report chemostratigraphic data ($\delta^{13}C$, $\delta^{18}O$, $\delta^{34}S_{CAS}$, $\delta^{34}S_{py}$, and trace element concentrations) of the Quanji Group. Together with previously published data from the Hankalchough Formation in the Quruqtagh area (NW China) and the Zhengmuguan Formation in North China, both of which contain glacial deposits considered to be equivalents of the Hongtiegou diamictite (Wang et al., 1981; Lu et al., 1985), this study adds to a growing chemostratigraphic database relevant to Ediacaran glaciations.

2. Regional geology

The Neoproterozoic sedimentary succession in the Chaidam Basin is represented by the Quanji Group, which sporadically crops out at Oulongbluq, Shihuigou, Quanjishan and Dayangtougou areas, and is best exposed in the Quanjishan area (Fig. 1). The stratigraphy of the Quanji Group was first studied by Zhu (1957a,b), and was later refined by Wang et al. (1980), Wang et al. (1981), and Wang and Chen (1983). The Quanjishan area is located in the northwestern Qinghai Province, northwest China. Geographically, it lies on the northern margin of the Chaidam Basin and is adjacent to the southern slope of the Qilian Mountain Range.

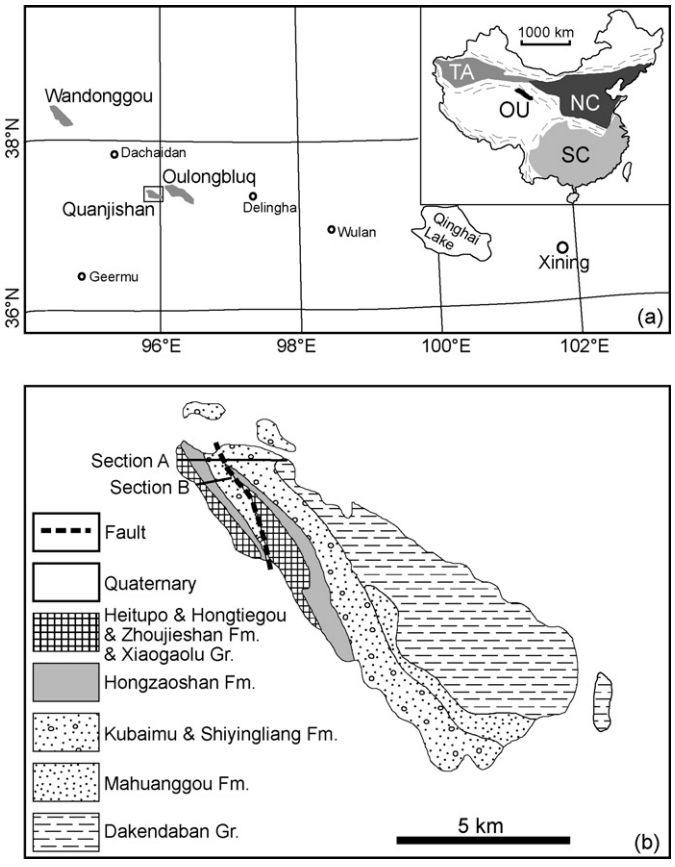

Fig. 1. (a) Outcrops of the Quanji Group (gray color) in the northern Chaidam Basin. Rectangled area is enlarged in b. Inset map shows the geographic location of the Oulongbluq microcontinent. TA: Tarim Block; NC: North China Block; SC: South China Block; OU: Oulongbluq microcontinent. (b) Geological map of the Quanjishan area. Sampled sections A and B are marked.

Geologically, the Quanjishan area belongs to the Oulongbluq microcontinent (Fig. 1) (Lu, 2002; Lu et al., 2007). The Oulongbluq microcontinent is one of the four minor tectonic units recognized between the Tarim and North China blocks. These four microcontinents are, from northeast to southwest, the Alashan, Qilian, Oulongbluq (or Quanji Massif), and Chaidam (Lu, 2002; Lu et al., 2007). They collided with one another to form a larger block during the late Silurian to early Devonian (Lu, 2002). The Oulongbluq microcontinent is approximately 500 km long, and extends in the northwest-to-southeast direction. It borders the Qilian and Chaidam microcontinents by the Zongwulong fault and the Shaliuhe–Yukahe eclogite zone, respectively.

3. Litho- and biostratigraphy of the Quanji Group

The basement of Oulongbluq microcontinent consists of the early Palaeoproterozoic Delingha gneiss, the late Palaeoproterozoic Dakendaban schist, and the Mesoproterozoic Wandonggou schist. The metamorphosed basement is unconformably covered by Neoproterozoic sedimentary sequence, the Quanji Group. In the Quanjishan area, the Quanji Group is represented by a ~1.5 km-thick siliciclastic-dominant succession that was probably deposited in a Neoproterozoic intra-cratonic aulacogen (Lu, 2002; Lu et al., 2007). Here, the Quanji Group unconformably overlies the late Palaeoproterozoic Dakendaban Group and underlies the early Cambrian Xiaogaolu Group (Wang et al., 1980). The Quanji Group is divided into 7 formations, in stratigraphic order, the Mahuanggou, Kubaimu, Shiyingliang, Hongzaoshan, Heitupo, Hongtiegou and Zhoujieshan formations (Fig. 2a) (Wang et al., 1980). These formations are briefly described below.

3.1. The Mahuanggou Formation

The Mahuanggou Formation is about 450-m thick, and unconformably overlies the late Palaeoproterozoic biotite and plagioclase schist of the Dakendaban Group. The lower part of the Mahuanggou Formation is composed of greenish-gray to purplish-gray, cross-bedded conglomerates. Clasts are well rounded and moderately to poorly sorted, and are composed of quartzite with minor volcanic and gneiss components. Conglomerates gradually grade into cross-bedded arkosic sandstone in the upper Mahuanggou Formation. The Mahuanggou Formation represents fluvial deposition on the Oulongbluq metamorphic basement (Wang et al., 1980).

3.2. The Kubaimu Formation

In the northwestern part of the Quanjishan area, the Mahuanggou Formation is missing and the Kubaimu Formation sits directly on the Dakendaban Group, whereas in the southeast, the 350-m thick Kubaimu Formation conformably overlies the Mahuanggou Formation (Fig. 1). Thus, the Mahuanggou–Kubaimu succession may represent an onlap sequence onto the underlying Mesoproterozoic metamorphic rock. The Kubaimu Formation is characterized by a fining upward sequence, and is divided into three lithological members. The lower member is dominated by conglomerate intercalated with quartzarenite with subaerial exposure structures (e.g. mudcrack casts). Clasts are well rounded and sorted, and mainly composed of quartzarenite, metavolcanic tuff, and porphyritic granite. Clasts content and size decrease upsection to light red quartzarenite of the middle member and medium- to fine-grained quartzarenite of the upper member. Cross-bedding, symmetrical and asymmetrical ripple marks are well developed in quartzarenite. The Kubaimu Formation represents a transgressive sequence from terrestrial fluvial, to terrestrial–marine transitional, to shallow marine environments (Wang et al., 1980).

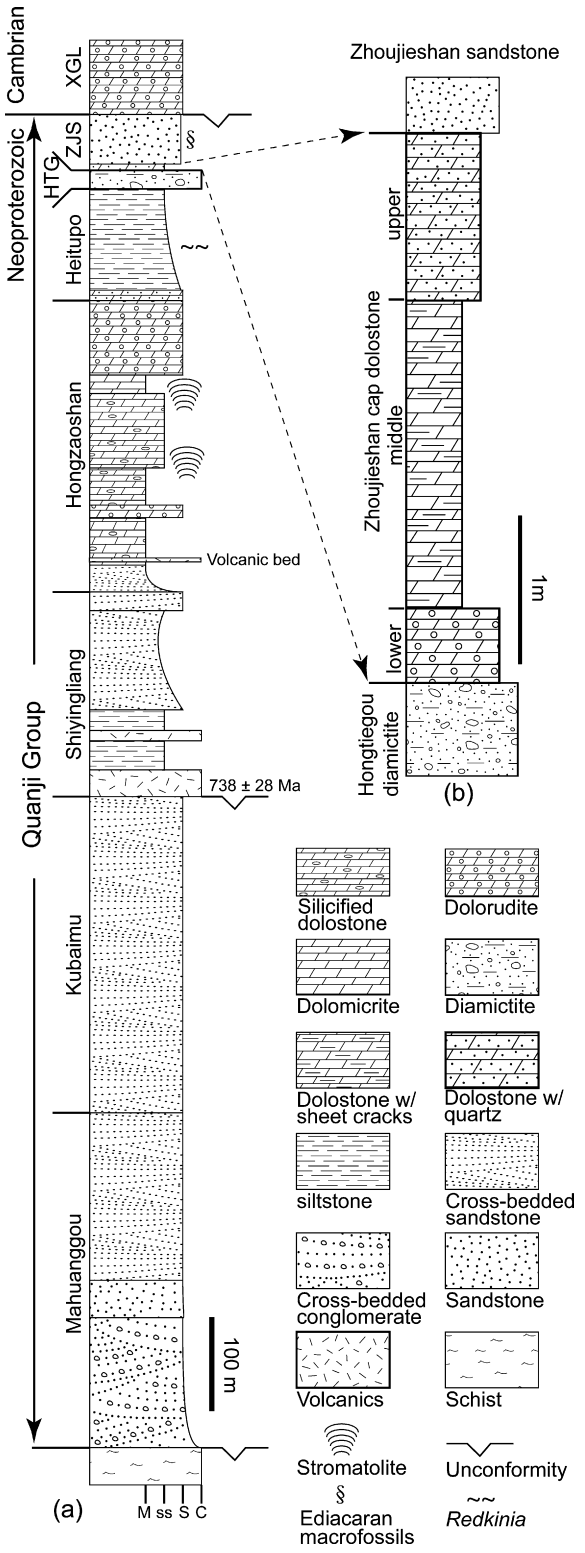

Fig. 2. (a) Stratigraphic column of the Quanji Group. HTG: Hongtiegou Formation; ZJS: Zhoujieshan Formation; XGL: Xiaogaolu Group. M: mudstone; ss: siltstone; S: sandstone; C: conglomerate. (b) Stratigraphic column of the Zhoujieshan cap dolostone at section B in the Quanjishan area.

3.3. The Shiyingliang Formation

The Shiyingliang Formation disconformably overlies the Kubaimu Formation, and is about 200-m thick in the Quanjishan area. The disconformity between the Kubaimu and Shiyingliang formations is cryptic in the Quanjishan area, but is represented by a prominent erosional surface in the Oulongbluq area (Wang et al., 1980). The Shiyingliang Formation begins with a 30-m thick greenish-gray basaltic andesite with lapilli stone. A 738 ± 26 Ma SHRIMP zircon U–Pb age has been obtained from this volcanic unit [(Lu, 2002), but later revised as 740 ± 16 Ma (Lu et al., 2007)]. This volcanic unit is succeeded by 30 m of siltstone and another volcanic unit consisting of 8-m thick yellowish-green basaltic and andesitic volcanics. The rest of the Shiyingliang Formation consists of light gray, thin to thick-bedded quartzite intercalated with yellowish-green thin-bedded siltstone. Cross stratification is well developed throughout the formation. Subaerial exposure structures (e.g. mudcrack casts) occur abundantly in the lower Shiyingliang Formation. The Shiyingliang Formation is another transgressive sequence following the depositional hiatus after the Kubaimu Formation.

3.4. The Hongzaoshan Formation

The transition from the Shiyingliang to Hongzaoshan Formation is gradational. The beginning of the Hongzaoshan Formation is marked by the first appearance of purplish, thin to medium-bedded tuffaceous sandstone (Fig. 3b). Mudcrack casts (Fig. 3c), halite pseudomorphs (Fig. 3d), and ripple marks are common in the lower Hongzaoshan Formation. The purple sandstones grade into finely laminated dolostones with thin chert beds. A 3-m thick greenish volcanic unit with lapilli (Fig. 3e) occurs within the laminated dolostone. The laminated dolostone is followed by ~230-m thick dark-gray to light-gray stromatolitic dolostone (Fig. 3f), laminated dolomicrite (Fig. 3g), and intraclastic dolorudite (Fig. 3h). The dolostone is typically recrystallized or silicified. Stromatolites have been identified as *Cryptozoon*, *Conophyton*, and *Katavia* (Wang et al., 1980). The Hongzaoshan Formation was deposited in a peritidal to shallow subtidal environment (Wang et al., 1980).

3.5. The Heitupo Formation

The Heitupo Formation in the Quanjishan area is about 120 m thick. The transition between the Hongzaoshan and the Heitupo formations is gradational. The lowest 10 m of the Heitupo Formation is composed of yellowish-green, thin to medium-bedded dolomicrite that gradually pass into green-gray siltstone. Several layers of hematite occur within the dolomicrite with a maximum thickness of 30 cm. The upper part of the Heitupo Formation is composed of greenish-gray, carbonaceous shale with sandstone concretions (Fig. 3i). The Heitupo Formation was deposited in lower subtidal environment. Tooth-shaped fossils described as scolecodonts (but probably representing fragments of *Redkinia*) have been reported from the Heitupo Formation (Wang et al., 1980), although a systematic paleontological description and biostratigraphic investigation of these fossils is needed. It is important to note that *Redkinia* was first reported from Redkino horizon in the East European Platform (Burzin, 1995), which is likely ~555 Ma (Martin et al., 2000; Vorob'eva et al., 2009).

3.6. The Hongtiegou Formation

The Hongtiegou Formation is ~18 m thick in the Quanjishan area, but has a maximum thickness of 75 m in the Shihuigou area. The Hongtiegou Formation consists of green, yellow, and purplish-red massive diamictite (Fig. 4a–d). The glacial origin of the Hongtiegou diamictite was first proposed by Sun (1959), and has been widely accepted by subsequent researchers (Wang et al., 1980; Wang and Chen, 1983). The transition from the Heitupo Formation to the Hongtiegou diamictite is gradational. In the Quanjishan area, the beginning of the Hongtiegou Formation is marked by the presences of pebbles in greenish muddy/silty matrix.

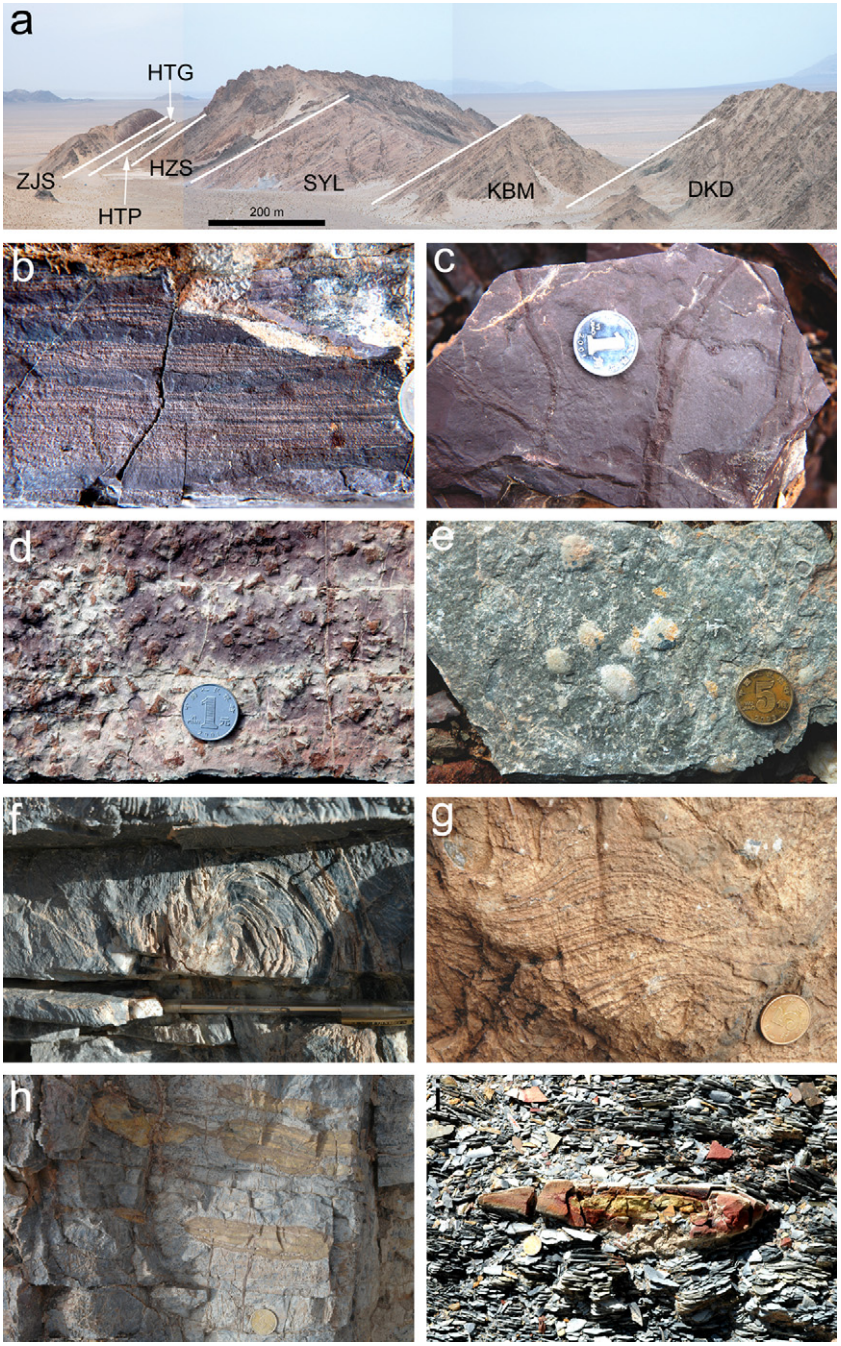

Fig. 3. (a) Field photograph of the Quanji Group at section A in the Quanjishan area. DKD: Dakendaban Group; KBM: Kubaimu Formation; SYL: Shiyingliang Formation; HZS: Hongzaoshan Formation; HTP: Heitupo Formation; HTG: Hongtiegou Formation; ZJS: Zhoujieshan Formation. (b) Purplish-red, thin-bedded, tuffaceous sandstone in the lower Hongzaoshan Formation. (c) Cast of mudcracks in the lower Hongzaoshan Formation. (d) Halite pseudomorphs in the lower Hongzaoshan Formation. (e) Volcanic sedimentary rock with lapilli in the lower Hongzaoshan Formation. (f) Silicified stromatolite in the Hongzaoshan Formation. (g) Thin-laminated dolostone in the Hongzaoshan Formation. (h) Dolorudite in the Hongzaoshan Formation. (i) Dark-gray siltstone/shale with sandstone concretion in the Heitupo Formation. Coins in e, g, h, and i are about 1.5 cm in diameter; coins in b, c, and d are about 2 cm in diameter; marker pen in f is about 14 cm.

With progressively larger and more abundant clasts, the typical Heitupo greenish-gray shales give way to massive diamictite of the Hongtiegou Formation. Most clasts are derived from the underlying Hongzaoshan dolostone, and some are from older sandstone, conglomerate, and metamorphic rocks. Clasts are angular and poorly sorted (Fig. 4d). The largest clast observed in the measured sections is ~30 cm in diameter (Fig. 4b), but some giant boulders of more than 2 m in diameter have been reported from other localities (Wang et al., 1980). Dropstones (Fig. 4c) and striated clasts [pl. I, Fig. 8 of Wang and Chen, 1983] are widely distributed in the Hongtiegou Formation, indicating a glacial origin.

3.7. The Zhoujieshan Formation

The Zhoujieshan Formation begins with a 4–6-m thick yellow to pink dolostone, the Zhoujieshan cap dolostone (Fig. 4a). In spite of the abrupt lithological change from the massive diamictite of the underlying Hongtiegou Formation to the Zhoujieshan cap dolostone, there is no significant sedimentary break between the Hongtiegou and Zhoujieshan formations. This interpretation is supported by two lines of evidence. First, no subaerial exposure surface or incision valley is present at the contact between the diamictite and cap dolostone. Second, at closer examination, the

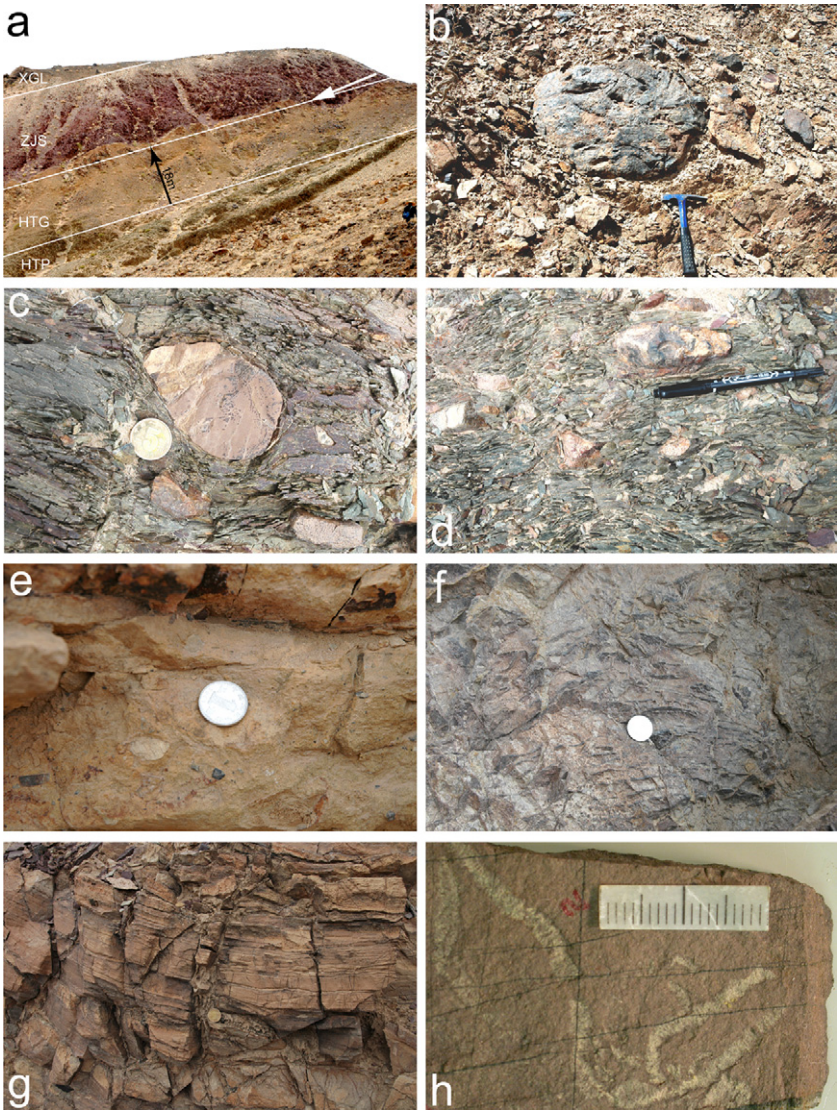

Fig. 4. (a) Field photograph of the Heitupo (HTP), Hongtiegou (HTG), Zhoujieshan (ZJS) formations, and Xiaogaolu Group (XGL) at section A. White arrow indicates the Zhoujieshan cap dolostone. (b) Out-sized clasts in the Hongtiegou diamictite. (c) Dropstone in the Hongtiegou diamictite. (d) The Hongtiegou diamictite. Note the poorly sorted clasts within greenish matrix. (e) Lower unit of the Zhoujieshan cap dolostone with dolomitic and siliciclastic clasts. (f) Dolostone with sheet-cracks in the middle Zhoujieshan cap dolostone. (g) Red dolomitic sandstone in the upper Zhoujieshan cap dolostone. (h) *Shaanxilithes ningqiangensis* from the Zhoujieshan sandstone. Coins in c and g are about 1.5 cm in diameter; coins in e and f are about 2 cm in diameter; hammer in b is about 30 cm long; marker pen in d is about 14 cm; scale bar in h in millimetric units.

lower 0.5 m of the Zhoujieshan cap dolostone contains siliciclastic and dolomitic clasts that are similar to clasts in the underlying diamictite (Figs. 2b and 4e), suggesting no significant change in the source of clasts. It is possible that the clasts in the lower unit of cap dolostone represent transgressive reworking at the top surface of unlithified diamictite, with simultaneous cementation during cap dolostone precipitation. It is interesting to note in passing that rare pebbly clasts are also present in the basal Doushantuo cap dolostone in South China (Jiang et al., 2006). The middle part of the cap Zhoujieshan dolostone is ~2.1 m thick, and consists of dolomicrite and dolomicrosparite with well-developed sheet-cracks filled with quartz (Fig. 4f). The upper unit is 1.2 m thick and is characterized by red dolomitic sandstone (Fig. 4g), with well rounded and moderately sorted quartz grains.

The upper unit of the Zhoujieshan cap dolostone gradually grades into the 50-m thick, red, thin-laminated siltstone/fine sandstone of the Zhoujieshan sandstone member. Abundant ribbon-shaped fossils have been discovered from the Zhoujieshan sandstone member. The first occurrence of these fossils, based on our field investigation, is only 5 m above the Zhoujieshan cap dolostone. These ribbon-shaped fossils were traditionally interpreted as trace fossils or *Sabellidites*-like tubular fossils (Wang et al., 1980; Xing et al., 1984). Systematic study of these fossils distinguishes two genera, *Shaanxilithes* (Fig. 4h) and *Helanoichnus*, both of which were interpreted as body fossils of unknown phylogenetic affinity (Shen et al., 2007). *Shaanxilithes* is a common fossil from the middle Dengying Formation (<551 Ma) in South China (Hua et al., 2000; Hua et al., 2004) and the upper Zhengmuguan Formation in North China (Li et al., 1997; Shen et al., 2007). *Helanoichnus* is known from the upper Zhengmuguan Formation as well (Yang and Zheng, 1985). Thus, the occurrence of *Shaanxilithes* and *Helanoichnus* in the Zhoujieshan sandstone implies a late Ediacaran age (<551 Ma) of the Zhoujieshan Formation. The Zhoujieshan sandstone member is disconformably overlain by the lower Cambrian Xiaogaolu Group that yields rare echinoderm fragments and hyolith fossils (Wang et al., 1980).

4. Methods

We investigated two sections in the Quanjishan area (labeled as section A and B in Fig. 1). At section A, we collected samples from the Zhoujieshan cap dolostone and the lower 80 m of the Hongzaoshan dolostone, because the upper part of the Hongzaoshan Formation is covered by talus. At section B, the Zhoujieshan cap dolostone and the upper 160 m of the Hongzaoshan Formation were sampled. Because of the close proximity of these two sections, they can be correlated using stratigraphic thickness and lithostratigraphic data. Sampling intervals were 1–4 m for the Hongzaoshan Formation and 0.1–0.5 m for the Zhoujieshan cap dolostone. We measured carbon and oxygen isotope compositions of all carbonate samples. In addition, sulfur isotope compositions of carbonate associated sulfate (CAS) and pyrite, and trace element concentrations (S, Fe, Mn, Sr) of the Zhoujieshan cap dolostone at section B were also analyzed.

4.1. Carbon and oxygen isotopes

Carbon and oxygen isotopes were analyzed in two laboratories. Samples from section A were prepared and analyzed in Nanjing Institute of Soil Science, Chinese Academy of Science. Small rock chips were cleaned and powdered. Rock powder (5 mg) was allowed to react with concentrated H_3PO_4 at 50 °C for 12 h, and CO_2 was extracted using traditional offline technique. Carbon and oxygen isotope ratios were measured on a Finnigan MAT 251 mass spectrometer. Analytical precision (1σ) is 0.1‰ for $\delta^{13}C$, and 0.3‰ for $\delta^{18}O$. Both $\delta^{13}C$ and $\delta^{18}O$ are reported as ‰ deviation from VPDB.

Samples from section B were prepared at Virginia Tech, and analyzed on a Micromass Isoprime dual-inlet gas source stable isotope mass spectrometer at University of Maryland, which is equipped with a peripheral Multiprep system for online carbonate reaction. Fresh carbonate samples were cut to make mirroring thin and thick sections. Powders were microdrilled from thick sections using a 1 mm drill bit. Microdrilling was guided by the petrographic observations of thin sections to avoid microveins and diagenetically altered areas. Analytical precision (1σ) is better than 0.1‰ for $\delta^{13}C$, and 0.3‰ for $\delta^{18}O$. Both $\delta^{13}C$ and $\delta^{18}O$ are reported as ‰ deviation from VPDB.

4.2. Sulfur isotope

Sulfur isotope compositions of disseminated pyrite and carbonate associated sulfate (CAS) were measured from the same rock samples where carbon and oxygen isotopes were analyzed. The procedure for CAS extraction followed (Shen et al., 2008). Rock chips (50–100 g) were washed by 3 M HCl to remove surface weathering products. Fresh samples were then crushed to 80 mesh, and leached with 10% NaCl for 24 h to remove soluble non-CAS sulfate. Pretreated samples were then dissolved following a stepwise acidification procedure (Shen et al., 2008). In the first treatment, each sample was immersed in 50 ml deionized water and 20 ml of 10 M HCl. It normally took about 30–60 min for reaction to complete. In subsequent treatments, 25 ml 10 M HCl was added each time until the carbonate component was quantitatively dissolved and no CO_2 bubbles were generated. After ~2 h, insoluble residue (mostly detrital component) was removed using 1 μ filter paper. Insoluble residue was carefully washed, dried, and weighed in order to quantify carbonate content (carbonate %) and calibrate trace element and CAS concentrations. The volume of supernatant was measured and then distributed into 50 ml centrifuge tubes, one of which was used for elemental analysis. 1–5 ml of $BaCl_2$ saturated aqueous solution was added to other tubes to precipitate sulfate as barite.

Disseminated pyrite was extracted using a modified chromium reduction method (Canfield et al., 1986; Goldberg et al., 2005; Shen et al., 2008). Five to seven grams of sample powder (80 mesh) was treated with 20 ml of 10 M HCl and 50 ml of 1 M $CrCl_2$ under a N_2 atmosphere. H_2S produced from pyrite reduction was bubbled through a 1 M zinc acetate trap to be precipitated as ZnS, which was then transferred to Ag_2S by reacting with $AgNO_3$ solution. Ag_2S was centrifuged, carefully washed using deionized water, and dried at 60 °C.

Sulfur isotopes were measured in the geochemistry laboratory at the University of Maryland. A Eurovector elemental analyzer (EA) was used for online combustion of barite and silver sulfide. The separation of SO_2 to a GV Isoprime mass spectrometer for $^{34}S/^{32}S$ analyses followed the procedures described in Grassineau et al. (2001). Barite and silver sulfide (~100 μg) were accurately weighed and folded into small tin cups with similar amount of V_2O_5. They were sequentially dropped with a pulsed 12 ml O_2 purge into a catalytic combustion furnace operating at 1030 °C. The frosted quartz reaction tube was packed with granular tungstic oxide on alumina ($WO_3 + Al_2O_3$) and high purity reduced copper wire for quantitative oxidation and O_2 resorption. Water was removed from the combustion products with a 10-cm magnesium perchlorate column, and the SO_2 was separated from other gases with a 0.8 m PTFE GC column packed with Porapak 50–80 mesh heated to 90 °C. The cycle time for these analyses was 210 s with reference gas injection as a 30-s pulse beginning at 20 s. Sample SO_2 pulses begin at 110 s and return to baseline values between 150 and 180 s, depending on sample size and column conditions. The effluent from the EA was introduced in a flow of He (80–120 ml/min) to the IRMS through a SGE splitter valve that controls the variable open split. Timed pulses of SO_2 reference gas (99.9% purity, ~3 nA) were introduced at the beginning of the run using an injector connected to the IRMS with a fixed open ratio split. The isotope ratios of reference and sample peaks were determined by monitoring ion beam intensities relative to background values. Isotope ratios are determined by comparing integrated peak areas of m/z 66 and 64 for the reference and sample SO_2 pulses, relative to the baseline of $\sim 1 \times 10^{-11}$ A. Isotopic results are expressed in the δ notation as per mil (‰) deviations from the VCDT standard. One sigma uncertainties of these measurements (±0.3‰ or better) were determined by multiple analyses of a standard barite (NBS 127) interspersed with the samples.

4.3. Elemental geochemistry

Trace elements (Fe, Mn, Sr, and S) were analyzed on an Inductively Coupled Plasma Atomic Emission Spectrometer (ICP-AES) in the Soil Testing Laboratory at Virginia Polytechnic Institute and State University. Solutions from CAS extraction were used for elemental analysis. Element concentrations were corrected for insoluble residue. CAS concentration was calculated from sulfur concentration. Analytical precision for elemental analyses was better than 5% as determined by repeated analyses of a standard solution with known concentration.

5. Results

5.1. $\delta^{13}C$ and $\delta^{18}O$

$\delta^{13}C$ and $\delta^{18}O$ in both sections are listed in Table 1 and Supplementary Table S1. The Hongzaoshan samples from section A and B represent the lower and upper part of Hongzaoshan Formation, respectively. $\delta^{13}C$ profile shows a positive shift from −5‰ to 0‰ in the lower Hongzaoshan Formation, and varies between −1‰ and +1‰ in the middle to upper Hongzaoshan dolostone (Fig. 5). $\delta^{18}O$ values of the Hongzaoshan Formation vary between −4.7‰ and −14.5‰. $\delta^{13}C$ values of the Zhoujieshan cap dolostone are similar in the two measured sections, with values between +0.5‰ and

Table 1
Geochemical data of the Zhoujieshan cap carbonate at section B in the Quanjishan area. ns., no sufficient yield; na., not analyzed.

Number	Height (m)	Fe (ppm)	Mn (ppm)	Sr (ppm)	CAS (ppm)	Mg/Ca	Carb.%	$\delta^{13}C$	$\delta^{18}O$		$\delta^{34}S_{CAS}$	$\delta^{34}S_{Pyrite}$	$\Delta^{34}S$
QJS-19	3.75	6839	2603	64	331	0.99	77	0.4		−4.1	14.9	ns.	na.
QJS-18	3.65	5433	1325	71	347	1.02	81	1.1		−4.9	14.3	23.2	−8.9
QJS-17	3.45	7694	1244	146	333	0.99	73	0.7		−3.7	16.8	25.4	−8.6
QJS-16	3.40	10,969	1746	137	580	0.93	73	0.8		−4.9	15.2	26.4	−11.2
QJS-15	3.10	10,960	2720	118	783	0.93	71	0.6		−4.3	14.6	24.3	−9.8
QJS-14	2.90	5850	1281	226	403	0.99	91	1.1		−5.4	15.2	21.7	−6.5
QJS-13	2.60	na.	na.	na.	na.	na.	na.	1.0		−4.7	ns.	ns.	na.
QJS-12	2.30	7008	2401	274	295	0.96	90	0.8		−5.5	17.6	22.4	−4.8
QJS-11	2.10	6470	1458	210	161	1.00	79	1.5		−4.9	22.2	15.2	7.0
QJS-10	1.90	3995	1958	195	134	1.03	97	0.8		−4.9	24.1	19.6	4.5
QJS-9	1.60	6188	1968	388	53	1.01	96	1.1		−4.1	ns.	16.9	na.
QJS-8	1.30	4264	1755	215	159	1.01	94	0.0		−5.9	ns.	18.8	na.
QJS-7	1.00	4475	1203	301	237	1.01	96	1.2		−3.4	17.2	14.6	2.6
QJS-6	0.70	7369	1501	329	530	1.00	93	0.8		−4.6	13.9	14.4	−0.5
QJS-5	0.55	6484	1420	371	134	1.01	91	1.7		−4.6	20.6	14.6	6.0
QJS-4	0.25	5575	1371	301	148	1.01	94	1.7		−3.6	ns.	14.5	na.
QJS-3	0.15	5157	1321	358	246	0.99	89	1.6		−4.6	ns.	13.6	na.
QJS-2	0.10	5607	1508	304	317	1.01	91	1.2		−4.8	14.9	12.9	2.0
QJS-1	0.00	5591	1249	255	185	0.99	92	1.7		−3.6	ns.	ns.	na.

+1.5‰ at section A, and between 0‰ and +1.7‰ at section B (Fig. 5). $\delta^{18}O$ values of the Zhoujieshan cap dolostone (−3.6‰ to −7.7‰) are greater and less variable than those of the Hongzaoshan Formation (Fig. 5).

5.2. $\delta^{34}S_{CAS}$ and $\delta^{34}S_{py}$

$\delta^{34}S_{CAS}$ and $\delta^{34}S_{py}$ values of the Zhoujieshan cap dolostone at section B are summarized in Table 1, and plotted in Fig. 6b. $\delta^{34}S_{CAS}$ values vary between +13.9‰ and +24.1‰, and do not show any stratigraphic trend. $\delta^{34}S_{py}$ profile displays a persistent positive stratigraphic trend from +12.9‰ to +26.4‰. The isotopic difference between CAS and pyrite ($\Delta^{34}S_{CAS-py} = \delta^{34}S_{CAS} - \delta^{34}S_{py}$) varies from −0.5‰ to +7.0‰ in the lower 2.3 m of the section, and decreases to negative values in the upper 1.5 m interval (−4.8‰ to −11.2‰).

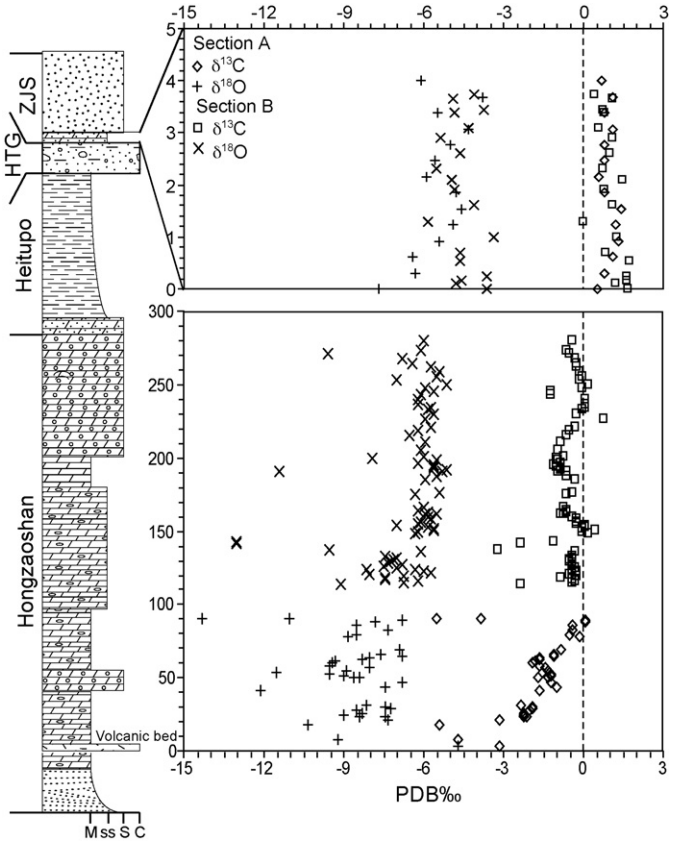

Fig. 5. Carbon and oxygen isotope profiles of the Hongzaoshan Formation and the Zhoujieshan cap dolostone. Samples from section A and section B (see Fig. 1) were analyzed by bulk and microdrilled samples, respectively. See Fig. 2 for lithological symbols. HTG: Hongtiegou Formation; ZJS: Zhoujieshan Formation.

5.3. Elemental geochemistry

Trace element (Fe, Mn, Sr and S) concentrations of the Zhoujieshan cap dolostone at section B are summarized in Table 1, and plotted in Fig. 6c and d. CAS concentration varies between 53 and 783 ppm (mean = 299 ppm; SD = 185 ppm), and shows a weak increasing trend. Mn concentration does not show any stratigraphic trend, and ranges from 1203 to 2720 ppm (mean = 1668 ppm; SD = 480 ppm). Fe concentration slightly increases upsection, and varies between 3995 and 10,969 ppm (mean = 6440 ppm; SD = 1935 ppm). Carbonate content (carbonate %, Fig. 6e) shows a sharp decrease in the upper cap dolostone unit, consistent with petrographic observation that the upper unit contains abundant quartz grains.

6. Discussions

6.1. Diagenetic alteration of $\delta^{13}C$ values

It is possible that $\delta^{13}C$ of Quanji samples has been modified as a result of diagenetic alteration. Since meteoric diagenetic alteration tends to reduce $\delta^{13}C$ values, the measured $\delta^{13}C$ represents a minimum estimate of the sedimentary value. Because both $\delta^{18}O$ and Mn/Sr are also altered during diagenesis, they are commonly used as diagenetic indicators for $\delta^{13}C$ (Kaufman and Knoll, 1995). It has been suggested that samples with Mn/Sr <10 and $\delta^{18}O > -5‰$ can be regarded as least altered, and their $\delta^{13}C$ values may approximate the primary sedimentary values (Kaufman and Knoll, 1995). Most samples from the Zhoujieshan cap dolostone have $\delta^{18}O$ values greater than −5‰ (Fig. 7a), and Mn/Sr ratios less than 10 (Fig. 7b), suggesting that $\delta^{13}C$ values of the Zhoujieshan cap dolostone are of chemostratigraphic significance.

However, $\delta^{18}O$ values of most Hongzaoshan samples range from −5‰ to −10‰, and show positive correlations with $\delta^{13}C$ values, suggesting that $\delta^{13}C$ values of most Hongzaoshan samples may have undergone alteration. It is interesting to note that $\delta^{18}O$ in section A is ~2‰ lower than that in section B. This difference may in part due to secular variation, diagenetic alteration, different sam-

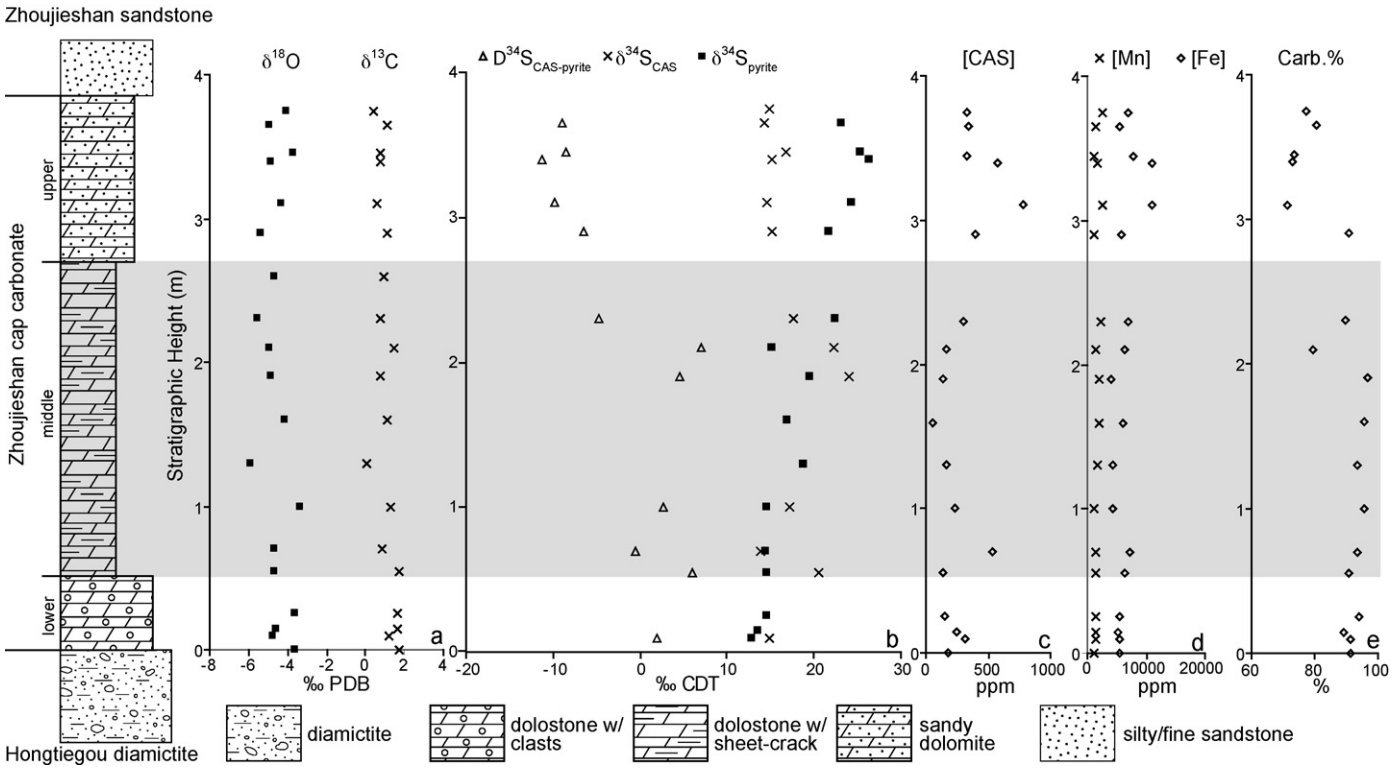

Fig. 6. Isotopic and elemental geochemistry profiles of the Zhoujieshan cap dolostone at section B. (a) $\delta^{13}C$ and $\delta^{18}O$; (b) $\delta^{34}S_{CAS}$, $\delta^{34}S_{py}$ and $\Delta^{34}S_{CAS-py}$ ($\delta^{34}S_{CAS} - \delta^{34}S_{py}$); (c) CAS concentration; (d) Fe and Mn concentrations; (e) carbonate content (carbonate%). Shading depicts the middle unit.

pling methods or analytical techniques (samples from section A were measured on bulk samples by offline reaction, whereas those from section B were measured on microdrilled powders by online reaction).

6.2. Fidelity of sulfur isotope signatures

Two sulfur components of the Zhoujieshan cap dolostone are considered in this study: carbonate associated sulfate (CAS) and

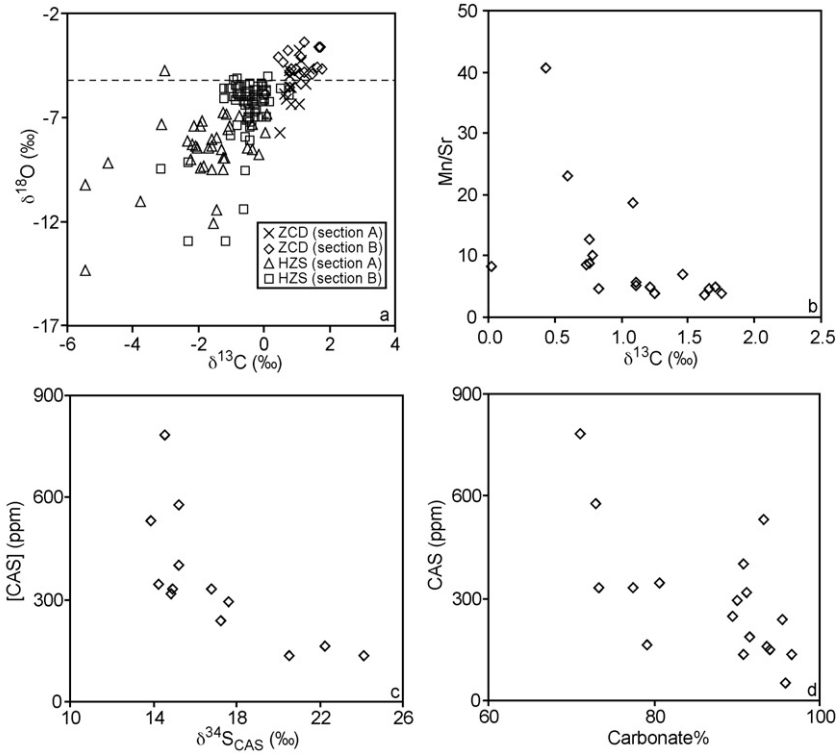

Fig. 7. Isotope and elemental crossplots. (a) $\delta^{13}C$–$\delta^{18}O$ crossplot. Dashed line marks $\delta^{18}O = -5‰$. (b) $\delta^{13}C$–Mn/Sr crossplot. (c) $\delta^{34}S_{CAS}$–[CAS] crossplot. (d) Carbonate%–[CAS] crossplot. ZCD: Zhoujieshan cap dolostone; HZS: Hongzaoshan dolostone.

disseminated pyrite. CAS is trace amount of sulfate that substitutes CO_3^{2-} within carbonate lattice (Pingitore et al., 1995), and $\delta^{34}S_{CAS}$ has been widely used as a useful proxy for the composition of seawater sulfate (Kampschulte et al., 2001; Kampschulte and Strauss, 2004; Bottrell and Newton, 2006). For example, CAS extracted from modern foraminifera tests yields an average $\delta^{34}S_{CAS}$ value of +20.6‰, which is comparable to $\delta^{34}S$ of modern seawater sulfate (Burdett et al., 1989).

However, possible diagenetic alteration of $\delta^{34}S_{CAS}$ should be considered, particularly for ancient samples. During diagenesis (e.g. dolomitization), CAS could be released from the crystal lattice of precursor carbonate minerals (e.g. aragonite, high-Mg calcite), and sulfate in pore water could be incorporated in stabilized carbonate minerals (e.g. low-Mg calcite, dolomite). The effect of dolomitization on $\delta^{34}S_{CAS}$ has not been completely understood yet, although it has been shown that sulfate loss during aragonite–calcite inversion does not have significant impact on $\delta^{34}S_{CAS}$ values (Lyons et al., 2004; Gellatly and Lyons, 2005). Comparison between Proterozoic dolostones and interbedded evaporites shows that $\delta^{34}S_{CAS}$ of dolostone is about 4‰ greater than $\delta^{34}S$ of coeval evaporite (Kah et al., 2004; Mazumdar and Strauss, 2006), suggesting incorporation of heavy sulfate from pore water during dolomitization. Thus, $\delta^{34}S_{CAS}$ from dolostone samples may represent a maximum estimate for seawater $\delta^{34}S_{sulfate}$. However, a recent study on Early Triassic carbonate and evaporate indicates that $\delta^{34}S_{CAS}$ of dolostone is identical to $\delta^{34}S_{sulfate}$ of intercalated evaporite, but $\delta^{34}S_{CAS}$ values of equivalent limestone from deeper water sections in the same basin are greater than those of dolostone (Marenco et al., 2008b). It was therefore suggested that dolomitization and evaporite formation in proximal environments was influenced by ^{34}S-depleted sulfate derived from continental weathering (Marenco et al., 2008b). Regardless, the similarity (within a few ‰) between $\delta^{34}S_{CAS}$ of dolostone and $\delta^{34}S_{sulfate}$ of intercalated evaporite implies that $\delta^{34}S_{CAS}$ might be buffered during dolomitization.

It is also possible that $\delta^{34}S_{CAS}$ could have been contaminated by non-CAS sulfate. For example, pyrite might be oxidized to sulfate during prolonged exposure in outcrop. In our analysis, sample powders were first treated with 10% NaCl solution for 24 h and washed by deionized water to remove non-CAS sulfates. NaCl solution greatly enhances the solubility of non-CAS sulfate, such as gypsum and sulfate derived from pyrite oxidation. The potential pyrite oxidation during acidification procedure is probably negligible in our analysis. Recent experiment shows that, in samples with low pyrite content (<1%) and relatively high $\delta^{34}S_{py}$ values (+9.4‰), pyrite oxidation during CAS extraction caused only a small negative shift (less than 4‰) in $\delta^{34}S_{CAS}$ (Marenco et al., 2008a). $\delta^{34}S_{py}$ values of Zhoujieshan cap dolostone are high (from +12.9‰ to +26.4‰), and pyrite concentrations are far less than 1%. Therefore, pyrite oxidation during CAS extraction is unlikely to have caused significant change in $\delta^{34}S_{CAS}$ values.

$\delta^{34}S_{py}$ was measured by the traditional chromium reduction method, which has been widely used to extract pyrite sulfur (Canfield et al., 1986). This extraction procedure does not introduce any significant isotopic fractionation. Control experiments by reducing pure pyrite to Ag_2S does not yield significant isotopic difference ($\delta^{34}S_{py}$ = +1.9‰ vs. $\delta^{34}S_{Ag2S}$ = +2.6‰) (Shen et al., 2008).

The origin of pyrite also matters. Pyrites in the Zhoujieshan cap dolostone are probably deposited within sediment pore space during early diagenesis. In the Zhoujieshan cap dolostone, most pyrites are small (<20 μm) subeuhedral crystals. They are randomly distributed within the dolomicrite or dolomicrosparite matrix, and are not associated with microveins. These observations imply that disseminated pyrites in the Zhoujieshan cap dolostone were not formed during late diagenesis. Instead, they were likely precipitated from pore water that was inherited from overlying seawater.

6.3. Age of the Hongtiegou glaciation

Because of the lack of direct radiometric dates and biostratigraphic constraints, the age and correlation of the Hongtiegou diamictite have long been controversial. It has been variably correlated with the ~635 Ma Nantuo glaciation in South China (Zhao et al., 1980), the Ediacaran Hankalchough glaciation in the Quruqtagh area (Wang et al., 1981; Lu et al., 1985), or regarded as a Cambrian glaciation (Wang et al., 1980). The only geochronological constraint on the Hongtiegou diamictite is a SHRIMP U–Pb zircon age of 738 ± 28 Ma from the basal Shiyingliang Formation (Lu, 2002; Lu et al., 2007). This age does not falsify any of the age interpretations proposed for the Hongtiegou Formation.

The presence of the late Ediacaran fossils *Helanoichnus* and *Shaanxilithes* in the Zhoujieshan sandstone, however, rules out the possibility that the underlying Hongtiegou diamictite could represent a Cambrian glaciation, although it does not falsify the Cryogenian or Ediacaran interpretations (Shen et al., 2007). Given that the lowest occurrence of *Helanoichnus* and *Shaanxilithes* in the Zhoujieshan sandstone is within 5 m above the Zhoujieshan cap dolostone and that there is no evidence for an unconformity between the Zhoujieshan Formation and the Hongtiegou Formation, the Hongtiegou diamictite is more likely of Ediacaran age. Moreover, the occurrence of Redkinia (~555 Ma based on biostratigraphic data from the East European Platform) in the underlying Heitupo Formation is inconsistent with a Cryogenian age, but supports a late Ediacaran age, for the Hongtiegou glaciation (Wang et al., 1980; Burzin, 1995). If so, the Hongtiegou glaciation may have occurred <15 million years before the Precambrian–Cambrian boundary.

In this study, we provide chemostratigraphic data that bear on the age of the Hongtiegou glaciation. The positive $\delta^{13}C$ values of the Zhoujieshan cap dolostone are intriguing. $\delta^{13}C$ data of cap carbonates above Ediacaran glacial diamictites are sparse, but existing data show wide variations. For example, $\delta^{13}C$ values of the Gaskiers cap carbonate are negative (Myrow and Kaufman, 1999), but cap carbonate overlying the Ediacaran Egan diamictite unit in NW Australia is characterized by variable $\delta^{13}C$ values between −2‰ and +2‰ (Corkeron, 2007). As another example, the Ediacaran Hankalchough cap carbonate [<615 ± 6 Ma; (Xu et al., 2009)] in the Quruqtagh area of NW China shows large spatial variations in $\delta^{13}C$ between 0‰ and −18‰ (Xiao et al., 2004). Thus, the variable $\delta^{13}C$ data of cap carbonates overlying Ediacaran glacial diamictites, which are in sharp contrast to the consistently negative $\delta^{13}C$ values of cap carbonates overlying the Marinoan glacial deposits, indicate that there may have been multiple regional glaciations in the Ediacaran Period, and/or there may have been strong geochemical heterogeneity in Ediacaran basins.

$\delta^{13}C$ data from the Hongzaoshan Formation can also provide chemostratigraphic constraints on the age of the Hongtiegou diamictite. $\delta^{13}C$ values of the Hongzaoshan Formation show a steady shift from −5‰ to ~0‰ in the lower 90 m, and vary between −1‰ and +1‰ in the upper 160 m. Given available biostratigraphic and geochronometric data from the Quanji Group, we speculate that the negative $\delta^{13}C$ excursion in the Hongzaoshan Formation may be equivalent to the negative excursion in the Shuiquan Formation (Xiao et al., 2004), which has been constrained between 615 ± 4 and 541 Ma (Xu et al., 2009).

The correlation of the Hongzaoshan negative $\delta^{13}C$ excursion with other regions is more elusive. In the Yangtze Gorges area of South China, there are three negative $\delta^{13}C$ excursions (~635 Ma EN1, EN2, and 551 Ma EN3) that are followed by periods of positive $\delta^{13}C$ values in the Doushantuo Formation (Zhou et al., 2004; Zhou and Xiao, 2007; McFadden et al., 2008). These three negative excursion intervals have been correlated with the post-Marinoan cap carbonate, the 582 Ma Gaskiers glaciation, and

the Shuram excursion, respectively (Condon et al., 2005). It is uncertain whether the negative $\delta^{13}C$ excursion in the Hongzaoshan dolostone can be correlated with EN1, EN2, or EN3 in South China. The Hongzaoshan–EN1 correlation is certainly possible, and it implies that the Hongzaoshan–Shuiquan correlation (see above) is not tenable. This correlation also implies a cryptic unconformity in the lower Hongzaoshan or Shiyingliang formations that would represent the Marinoan glaciation, but such an unconformity has not been recognized in field. Further, this correlation implies that the unique sedimentary structures associated with many cap dolostones overlying Marinoan glacial diamictites, such as seafloor precipitates and tube stones, are absent from the Hongzaoshan "cap carbonate". Although the issue remains unresolved, we tentatively favor the alternative correlation of the Hongzaoshan negative excursion with either the EN2 or EN3 excursion in South China. This preferred correlation implies that the Hongtiegou glaciation is younger than the 580 Ma Gaskiers glaciation or even younger than the 551 Ma EN3 excursion, the latter of which has been correlated with the Shuram excursion.

Ediacaran glacial deposits, although not as widely distributed as Marinoan-age glacial deposits, have been reported from several continents. Potential Ediacaran glacial deposits include the Zhengmuguan and Luoquan diamictites in North China (Li, 1980; Guan et al., 1986), the Hankalchough diamictite in the Quruqtagh area of NW China (Xiao et al., 2004), the Gaskiers diamictite in Newfoundland (Bowring et al., 2003), the Squantum tillite member in the Boston basin (Thompson and Bowring, 2000), the Mortensnes diamictite in northern Norway (Halverson et al., 2005), the Moelv diamictite in south Norway (Bingen et al., 2005), the Egan tillite and its equivalents in Australia (Corkeron, 2007), the Fersiga diamictite in western Africa (Bertrand-Sarfati et al., 1995), and the Baykonur diamictite in Kazakhstan and Kyrgystan (Chumakov, 2009). Most of these Ediacaran glacial deposits are not tightly constrained by radiometric dates so it is uncertain whether they represent one or more Ediacaran glaciations. Tentative chemostratigraphic correlation as outlined above, however, implies that there may have been multiple (and perhaps regional) Ediacaran glaciations and that the late Ediacaran is not characterized by supergreenhouse climatic conditions.

6.4. Geochemical cycle after the Hongtiegou glaciation

The Zhoujieshan cap dolostone immediately overlies the Hongtiegou glacial deposit without any evidence for a sedimentary break. Therefore, it may record the ocean chemistry in the Oulongbluq basin following the Hongtiegou glaciation. In this section we describe a geochemical model to explain the $\delta^{13}C$, $\delta^{34}S_{CAS}$, and $\delta^{34}S_{py}$ values of the Zhoujieshan cap dolostone.

6.4.1. Interpretation of $\delta^{13}C$ in the Zhoujieshan cap dolostone

Precipitation of cap carbonate after glaciations requires a source of seawater alkalinity. In explaining the negative $\delta^{13}C$ features of the cap carbonate overlying Marinoan-age glacial deposits, a number of hypotheses have been proposed to account for the source of ^{12}C-enriched alkalinity. In the snowball Earth model, ^{12}C-enriched alkalinity is hypothesized to have come from post-glacial chemical weathering of silicate rock (Hoffman et al., 1998). Alternative source of ^{12}C-enriched alkalinity could have derived from oxidation of fossil organic matter (Kaufman et al., 2007), destabilization and anaerobic oxidation of gas hydrate (Kennedy et al., 2001; Jiang et al., 2003; Wang et al., 2008), or upwelling of deep waters (Grotzinger and Knoll, 1995).

In contrast to the pervasively negative $\delta^{13}C$ values of cap carbonates overlying Marinoan-age glacial diamictites (Halverson, 2006; Jiang et al., 2006), the Zhoujieshan cap dolostone has distinctively positive $\delta^{13}C$ values (Figs. 5 and 6a). The positive $\delta^{13}C$ values imply that the aforementioned ^{12}C-enriched alkalinities did not have a significant impact on the carbon cycles in the post-glacial Oulongbluq basin. Additional factors that may have contributed to the positive $\delta^{13}C$ values of the Zhoujieshan cap dolostone include (1) enhanced weathering of carbonate rocks (as opposed to siliciclastic rocks) (Higgins and Schrag, 2003); (2) strong evaporation in a restricted basin; and/or (3) post-glacial resumption of the biological pump. Regardless of the responsible geochemical processes, the Zhoujieshan cap dolostone is characterized by carbon isotope values that are similar to Phanerozoic normal marine carbonates but drastically different from cap carbonate overlying Marinoan glacial diamictites. This suggests that the Hongtiegou glaciation had much less geochemical consequences than the Marinoan glaciation.

6.4.2. Interpretation of sulfur isotopes

Sulfur isotopes of the Zhoujieshan cap dolostone have three distinctive features: (1) $\delta^{34}S_{CAS}$ shows rapid stratigraphic fluctuations, particularly in the lower and middle units of the Zhoujieshan cap dolostone, ranging from +13.9‰ and +24.1‰; (2) $\delta^{34}S_{CAS}$ and $\delta^{34}S_{py}$ are decoupled (i.e. $\delta^{34}S_{CAS}$ and $\delta^{34}S_{py}$ do not covary; instead, $\delta^{34}S_{py}$ increases steadily from +12.9‰ to +26.4‰ in the Zhoujieshan cap dolostone); (3) dolomitic sandstone of the upper unit shows inverse fractionation between CAS and pyrite ($\Delta^{34}S_{CAS-py} = \delta^{34}S_{CAS} - \delta^{34}S_{py} < 0$).

The rapid stratigraphic variation in $\delta^{34}S_{CAS}$ suggests a generally low-sulfate concentration in the surface water of Oulongbluq basin after the Hongtiegou glaciation. Although it is hypothesized that seawater sulfate concentrations increased to near modern levels during the Ediacaran Period (Hurtgen et al., 2002; Fike et al., 2006; Halverson and Hurtgen, 2007), recent studies indicate that seawater sulfate concentrations were geographically variable and in some basins may have remained relatively low until 551 Ma (McFadden et al., 2008) or until the Precambrian/Cambrian boundary (Ries et al., 2009). A small sulfate reservoir, particularly coupled with a restricted basin, means that the isotopic composition of sulfate is more susceptible to external perturbations (Kah et al., 2004; Shen et al., 2008). Also, a small sulfate reservoir would be more susceptible to local perturbations, thus leading to greater spatial heterogeneity (McFadden et al., 2008; Ries et al., 2009). Thus, the stratigraphic and spatial variations in $\delta^{34}S_{CAS}$ of Ediacaran rocks indicate generally low oceanic sulfate concentrations, despite evidence for episodic oceanic oxidation and increase in oceanic sulfate concentration in the Ediacaran Period (Fike et al., 2006; McFadden et al., 2008).

In the dolomitic sandstone of the upper unit, $\delta^{34}S_{CAS}$ values become lower and less variable (between +14.3‰ and +16.8‰), while CAS concentrations (between 331 and 783 ppm) and quartz grain content are both higher than the lower and middle units (Fig. 6). This relationship is also reflected in the negative correlation between CAS concentration and $\delta^{34}S_{CAS}$ (Fig. 7c). We interpret this relationship as evidence for increasing terrestrial sulfate input into the Oulongbluq basin, which introduced more quartz grains and more sulfate derived from pyrite oxidation, the latter of which was sufficient enough to have an impact on the relatively small surface ocean sulfate reservoir.

In modern oceans, $\delta^{34}S_{CAS}$ and $\delta^{34}S_{py}$ are coupled via bacteria sulfate reduction. In this reaction, sulfate reducing bacteria preferentially reduces $^{32}SO_4^{2-}$ to hydrogen sulfide (H_2S), which in term reacts with reactive Fe^{2+} to precipitate pyrite. Thus, $\delta^{34}S_{py}$ is expected to be lower than contemporaneous $\delta^{34}S_{sulfate}$ (Shen and Buick, 2004). In a steady state open system where the fractionation factor between sulfate and sulfide is held constant, $\delta^{34}S_{py}$ and $\delta^{34}S_{sulfate}$ are expected to covary linearly. In a real sedimentary system, however, pyrite precipitation often occurs within pore water, which can be regarded as a closed system depending on the relative rates of sulfate consumption and supply. In a closed system, resid-

ual sulfate becomes increasingly heavy as a consequence of sulfate reduction, and instantaneous $\delta^{34}S_{py}$ values would also increase progressively and might exceed the initial sulfate $\delta^{34}S$ value. However, the cumulative $\delta^{34}S_{py}$ should always be lower than the initial sulfate $\delta^{34}S$ value, and positive $\Delta^{34}S_{CAS-py}$ values are expected.

The Zhoujieshan cap dolostone, however, shows neither $\delta^{34}S_{CAS} - \delta^{34}S_{py}$ co-variation nor positive $\Delta^{34}S_{CAS-py}$ values. We interpret this unusual sulfur isotope data using a stratification model (Shen et al., 2008; Giddings and Wallace, 2009a,b), in which CAS and pyrite were derived, respectively from the surface and deep waters that had distinct sulfur isotope signatures. We speculate that the Oulongbluq basin was a restricted basin and became stratified after the Hongtiegou glaciation, and that the Zhoujieshan cap dolostone at the measured section was deposited below the chemocline. In this model, the cap dolostone was derived pelagically from surface ocean DIC, and CAS was derived from surface water sulfate. Because of the small oceanic sulfate reservoir, surface water sulfate was influenced strongly by terrestrial input, leading to stratigraphically variable $\delta^{34}S_{CAS}$ values. $\delta^{13}C$ values, however, are not as variable, possibly because of the buffering effect of a relatively large DIC reservoir in the surface ocean, basin restriction, and/or post-glacial resumption of biological productivity.

Pyrite, on the other hand, was precipitated within sedimentary pore water. The sulfur source for bacterial sulfate reduction came from the anoxic bottom water. Because of stratification, sulfate concentration in the bottom water decreased and sulfur isotope increased progressively due to Rayleigh distillation in a closed system. This model can explain the steady stratigraphic increase in $\delta^{34}S_{py}$ of the Zhoujieshan cap dolostone, eventually leading to $\delta^{34}S_{py}$ values greater than $\delta^{34}S_{CAS}$ values in the upper unit.

Recently, an intriguing model has been proposed to explain superheavy $\delta^{34}S_{py}$ values and negative $\Delta^{34}S_{CAS-py}$ ($=\delta^{34}S_{CAS} - \delta^{34}S_{py}$) values (Ries et al., 2009). Based on experimental data that aerobic oxidation of H_2S through biological and abiotic processes yields SO_4^{2-} and other oxidized species of sulfur that are depleted in ^{34}S (relative to the parent H_2S) by 4–18‰, Ries and colleagues argue that, when mass-dependent fractionation during bacterial sulfate reduction was minimal due to low seawater [SO_4^{2-}], oxidative fractionation of sulfur isotopes could enrich $\delta^{34}S_{H2S}$ relative to $\delta^{34}S_{SO4}$ via Rayleigh-type distillation (Ries et al., 2009). This model is particularly attractive given the low-sulfate concentration in some Ediacaran basins and the transitional but fluctuating redox conditions during the Ediacaran Period, and oxidative fractionation of sulfur isotopes may have also contributed to the negative $\Delta^{34}S_{CAS-py}$ values in the upper part of the Zhoujieshan cap dolostone.

7. Conclusions

The Neoproterozoic Quanji Group in the Chaidam Basin is a siliciclastic-dominated sequence with two carbonate units, the Hongzaoshan dolostone and the Zhoujieshan cap dolostone, the latter of which overlies the Hongtiegou glacial diamictite. Paleontological and chemostratigraphic data imply that the Hongtiegou diamictite represents an Ediacaran glaciation, possibly postdating the Gaskiers glaciation or even the Shuram event. Thus, multiple (and likely regional) glaciations may have occurred in the Ediacaran Period, and some may have occurred near the Precambrian–Cambrian boundary (Chumakov, 2009).

The Zhoujieshan cap dolostone is characterized by positive $\delta^{13}C$ values (0‰ to +1.7‰) and stratigraphically variable $\delta^{34}S_{CAS}$ values (between +13.9‰ and +24.1‰). $\delta^{34}S_{py}$ values, however, show a steady stratigraphic increase from +12.9‰ to +26.4‰. $\delta^{34}S_{py}$ and $\delta^{34}S_{CAS}$ values do not covary and, in the upper part of the Zhoujieshan cap dolostone, $\delta^{34}S_{py}$ values are greater than $\delta^{34}S_{CAS}$ values, resulting in inverse fractionations ($\Delta^{34}S_{CAS-py} < 0$).

The positive $\delta^{13}C$ values imply that the Hongtiegou glaciation had less impact on the carbon cycle than the Marinoan glaciations. Speculatively, basin restriction, evaporation, DIC buffering, carbonate rock weathering, and post-glacial resumption of biological productivity may have contributed to the positive $\delta^{13}C$ values seen in the Zhoujieshan cap dolostone. The stratigraphically variable $\delta^{34}S_{CAS}$ and negative $\Delta^{34}S_{CAS-py}$ of the Zhoujieshan cap dolostone can be interpreted as consequences of a restricted and stratified basin with relatively low-sulfate concentration in the aftermath of the Hongtiegou glaciation. In the stratified Oulongbluq basin, carbonate and CAS were derived from surface water, whereas sulfur source for sulfate reduction and pyrite precipitation was ultimately derived from bottom water. The surface water was influenced by terrestrial runoff, leading to variable $\delta^{34}S_{CAS}$ values due to the generally low oceanic sulfate concentrations. In contrast, Rayleigh distillation gradually depleted the deep water sulfate pool and made deep water sulfate increasingly heavy, eventually leading to $\delta^{34}S_{py}$ values greater than $\delta^{34}S_{CAS}$ derived from the surface water. Additionally, aerobic oxidation of sulfide in low-sulfate environments may also have contributed to the negative $\Delta^{34}S_{CAS-py}$ values of the Zhoujieshan cap dolostone (Ries et al., 2009).

Acknowledgements

This research was supported by grants from the US National Science Foundation, the National Natural Science Foundation of China, the Chinese Academy of Sciences, and the Chinese Ministry of Science and Technology. We thank Luyi Zhang and Yunshan Wang for field guidance; Nizhou Han and Juan Liu for technical help; Huiming Bao for useful discussion; and Ganqing Jiang and Tony Prave for constructive reviews.

Appendix A. Supplementary data

Supplementary data associated with this article can be found, in the online version, at doi:10.1016/j.precamres.2009.12.006.

References

Allen, A.P., Brown, J.H., Gillooly, J.F., 2002. Global biodiversity, biochemical kinetics, and the energetic-equivalence rule. Science 297, 1545–1548.
Bertrand-Sarfati, J., Moussine-Pouchkine, A., Amard, B., Ait Kaci Ahmed, A., 1995. First Ediacaran fauna found in western Africa and evidence for an Early Cambrian glaciation. Geology 23, 133–136.
Bingen, B., Griffin, W.L., Torsvik, T.H., Saeed, A., 2005. Timing of Late Neoproterozoic glaciation on Baltica constrained by detrital zircon geochronology in the Hedmark Group, south-east Norway. Terra Nova 17, 250–258.
Bottrell, S.H., Newton, R.J., 2006. Reconstruction of changes in global sulfur cycling from marine sulfate isotopes. Earth Science Reviews 75, 59–83.
Bowring, S., Myrow, P., Landing, E., Ramezani, J., Grotzinger, J., 2003. Geochronological constraints on terminal Neoproterozoic events and the rise of metazoans. Geophysical Research Abstracts 5, 13219.
Burdett, J., Authur, M., Richardson, M., 1989. A Neogene seawater sulfur isotope age curve from calcareous pelagic microfossils. Earth and Planetary Science Letters 94, 189–198.
Burzin, M.B., 1995. Late Vendian helicoid filamentous microfossils. Paleontological Journal 29, 1–34.
Canfield, D.E., Raiswell, R., Westrich, J.T., Reaves, C.M., Berner, R.A., 1986. The use of chromium reduction in the analysis of reduced inorganic sulfur in sediments and shales. Chemical Geology 54, 149–155.
Chumakov, N.M., 2009. The Baykonurian Glaciohorizon of the Late Vendian. Stratigraphy and Geological Correlation 17, 373–381.
Condon, D., et al., 2005. U–Pb ages from the Neoproterozoic Doushantuo Formation, China. Science 308, 95–98.
Corkeron, M., 2007. 'Cap carbonates' and Neoproterozoic glacigenic successions from the Kimberley region, north-west Australia. Sedimentology 54, 871–903.
Fanning, C.M., Link, P.K., 2004. U-Pb SHRIMP ages of Neoproterozoic (Sturtian) glaciogenic Pocatello Formation, southeastern Idaho. Geology 32, 881–884.
Fike, D.A., Grotzinger, J.P., Pratt, L.M., Summons, R.E., 2006. Oxidation of the Ediacaran ocean. Nature 444, 744–747.
Frimmel, H.E., Kloetzli, U.S., Siegfried, P.R., 1996. New Pb–Pb single zircon age constraints on the timing of Neoproterozoic glaciation and continental break-up in Namibia. Journal of Geology 104, 459–469.

Gellatly, A.M., Lyons, T.W., 2005. Trace sulfate in mid-Proterozoic carbonates and the sulfur isotope record of biospheric evolution. Geochimica et Cosmochimica Acta 69, 3813–3829.
Giddings, J.A., Wallace, M.W., 2009a. Facies-dependent $\delta^{13}C$ variation from a Cryogenian platform marginSouth Australia: Evidence for stratified Neoproterozoic oceans? Palaeogeography Palaeoclimatology Palaeoecology 271, 196–214.
Giddings, J.A., Wallace, M.W., 2009b. Sedimentology and C-isotope geochemistry of the Šturtiančap carbonate. South Australia. Sedimentary Geology 216, 1–14.
Goldberg, T., Poulton, S.W., Strauss, H., 2005. Sulphur and oxygen isotope signatures of late Neoproterozoic to early Cambrian sulphate, Yangtze Platform China: Diagenetic constraints and seawater evolution. Precambrian Research 137, 223–241.
Grassineau, N.V., Mattey, D.P., Lowry, D., 2001. Sulfur isotope analysis of sulfide and sulfate minerals by continuous flow-isotope ratio mass spectrometry. Analytical Chemistry 73, 220–225.
Grotzinger, J.P., Knoll, A.H., 1995. Anomalous carbonate precipitates: is the Precambrian the key to the Permian? Palaios 10, 578–596.
Guan, B., Wu, R., Hambrey, M.J., Geng, W., 1986. Glacial sediments and erosional pavements near the Cambrian–Precambrian boundary in western Henan Province, China. Journal of the Geological Society, London 143, 311–323.
Halverson, G.P., 2006. A Neoproterozoic chronology. In: Xiao, S., Kaufman, A.J. (Eds.), Neoproterozoic Geobiology and Paleobiology. Springer, Dordrecht, Netherlands, pp. 232–271.
Halverson, G.P., Hoffman, P.F., Schrag, D.P., Maloof, A.C., Rice, A.H.N., 2005. Toward a Neoproterozoic composite carbon-isotope record. Geological Society of America Bulletin 117, 1181–1207.
Halverson, G.P., Hurtgen, M.T., 2007. Ediacaran growth of the marine sulfate reservoir. Earth and Planetary Science Letters 263, 32–44.
Higgins, J.A., Schrag, D.P., 2003. Aftermath of a snowball Earth. Geochemistry, Geophysics, Geosystems (G3), doi:10.1029/2002GC000403.
Hoffman, P.F., Kaufman, A.J., Halverson, G.P., Schrag, D.P., 1998. A Neoproterozoic snowball Earth. Science 281, 1342–1346.
Hoffmann, K.-H., Condon, D.J., Bowring, S.A., Crowley, J.L., 2004. U-Pb zircon date from the Neoproterozoic Ghaub Formation Namibia: Constraints on Marinoan glaciation. Geology 32, 817–820.
Hua, H., Chen, Z., Zhang, L., 2004. *Shaanxilithes* from lower Taozichong Formation, Guizhou Province and its geological and paleobiological significance. Journal of Stratigraphy 28, 265–269.
Hua, H., Zhang, L., Zhang, Z., Wang, J., 2000. New fossil evidence from latest Neoproterozoic Gaojiashan biota, south Shaanxi. Acta Palaeontologica Sinica 39, 381–390.
Hurtgen, M.T., Arthur, M.A., Suits, N.S., Kaufman, A.J., 2002. The sulfur isotopic composition of Neoproterozoic seawater sulfate: implications for a snowball Earth? Earth and Planetary Science Letters 203, 413–429.
Jiang, G., Kennedy, M.J., Christie-Blick, N., 2003. Stable isotopic evidence for methane seeps in Neoproterozoic postglacial cap carbonates. Nature 426, 822–826.
Jiang, G., Kennedy, M.J., Christie-Blick, N., Wu, H., Zhang, S., 2006. Stratigraphy, sedimentary structures, and textures of the Late Neoproterozoic Doushantuo cap carbonate in South China. Journal of Sedimentary Research 76, 978–995.
Kah, L.C., Lyons, T.W., Frank, T.D., 2004. Low marine sulphate and protracted oxygenation of the Proterozoic biosphere. Nature 431, 834–838.
Kampschulte, A., Bruckschen, P., Strauss, H., 2001. The sulphur isotopic composition of trace sulphates in Carboniferous brachiopods: implications for coeval seawater, correlation with other geochemical cycles and isotope stratigraphy. Chemical Geology 205, 149–173.
Kampschulte, A., Strauss, H., 2004. The sulfur isotopic evolution of Phanerozoic seawater based on the analysis of structurally substituted sulfate in carbonates. Chemical Geology 204, 255–286.
Kaufman, A.J., Corsetti, F.A., Varni, M.A., 2007. The effect of rising atmospheric oxygen on carbon and sulfur isotope anomalies in the Neoproterozoic Johnnie Formation, Death Valley, USA. Chemical Geology 237, 47–63.
Kaufman, A.J., Knoll, A.H., 1995. Neoproterozoic variations in the C-isotope composition of sea water: stratigraphic and biogeochemical implications. Precambrian Research 73, 27–49.
Kendall, B., Creaser, R.A., Selby, D., 2006. Re-Os geochronology of postglacial black shales in Australia: constraints on the timing of "Sturtian" glaciation. Geology 34, 729–732.
Kennedy, M.J., Christie-Blick, N., Sohl, L.E., 2001. Are Proterozoic cap carbonates and isotopic excursions a record of gas hydrate destabilization following Earth's coldest intervals? Geology 29, 443–446.
Li, Q., 1980. Sinian Suberathem in the Minor Qinling Range in Shaanxi province. In: Tianjin Institute of Geology Mineral Resources (Ed.), Research in Precambrian Geology, Sinian Suberathem in China. Tianjin Science and Technology Press, Tianjin, pp. 314–331.
Li, R., Yang, S., Li, W., 1997. Trace Fossils from Sinian–Cambrian Boundary Strata in China. Geological Publishing House, Beijing, 99 pp.
Lu, S., 2002. The Precambrian Geology of Northern Tibet. Geological Publishing House, Beijing, 125 pp.
Lu, S., Li, H., Zhang, C., Niu, G., 2007. Geological and geochronological evidence for the Precambrian evolution of the Tarim Craton and surrounding continental fragments. Precambrian Research 160, 94–107.
Lu, S., Ma, G., Gao, Z., Lin, W., 1985. Sinian ice ages and glacial sedimentary facies-areas in China. Precambrian Research 29, 53–63.
Lyons, T.W., Walter, L.M., Gellatly, A.M., Martini, A.M., Blake, R.E., 2004. Sites of anomalous organic remineralization in the carbonate sediment of South Florida, USA: The sulfur cycle and carbonate-associated sulfate. In: Amend, J.P., Edwards, K.J., Lyons, T.W. (Eds.), Sulfur Biogeochemistry: Past and Present (GSA Special Paper 379). Geological Society of America, Boulder, Colorado, pp. 161–176.
Marenco, P.J., Corsetti, F.A., Hammond, D.E., Kaufman, A.J., Bottjer, D.J., 2008a. Oxidation of pyrite during extraction of carbonate associated sulfate. Chemical Geology 247, 124–132.
Marenco, P.J., Corsetti, F.A., Kaufman, A.J., Bottjer, D.J., 2008b. Environmental and diagenetic variations in carbonate associated sulfate: an investigation of CAS in the Lower Triassic of the western USA. Geochimica et Cosmochimica Acta 72, 1570–1582.
Martin, M.W., et al., 2000. Age of Neoproterozoic bilaterian body and trace fossils, White Sea, Russia: implications for metazoan evolution. Science 288, 841–845.
Mazumdar, A., Strauss, H., 2006. Sulfur and strontium isotopic compositions of carbonate and evaporite rocks from the late Neoproterozoic–early Cambrian Bilara Group (Nagaur-Ganganagar Basin, India): constraints on intrabasinal correlation and global sulfur cycle. Precambrian Research 149, 217–230.
McFadden, K.A., et al., 2008. Pulsed oxidation and biological evolution in the Ediacaran Doushantuo Formation. Proceedings of the National Academy of Sciences 105, 3197–3202.
Myrow, P.M., Kaufman, A.J., 1999. A newly discovered cap carbonate above Varanger-aged glacial deposits in Newfoundland, Canada. Journal of Sedimentary Research 69, 784–793.
Pingitore Jr., N.E., Meitzner, G., Love, K.M., 1995. Identification of sulfate in natural carbonates by X-ray absorption spectroscopy. Geochimica et Cosmochimica Acta 59, 2477–2483.
Ries, J.B., Fike, D.A., Pratt, L.M., Lyons, T.W., Grotzinger, J.P., 2009. Superheavy pyrite ($\delta^{34}S_{pyr} > \delta^{34}S_{CAS}$) in the terminal Proterozoic Nama Group, southern Namibia: a consequence of low seawater sulfate at the dawn of animal life. Geology 37, 743–746.
Shen, B., Xiao, S., Dong, L., Zhou, C., Liu, J., 2007. Problematic macrofossils from Ediacaran successions in the North China and Chaidam blocks: implications for there evolutionary root and biostratigraphic significance. Journal of Paleontology 81, 1396–1411.
Shen, B., et al., 2008. Stratification and mixing of a post-glacial Neoproterozoic ocean: evidence from carbon and sulfur isotopes in a cap dolostone from northwest China. Earth and Planetary Science Letters 265, 209–228.
Shen, Y., Buick, R., 2004. The antiquity of microbial sulfate reduction. Earth-Science Reviews 64, 243–272.
Sun, D., 1959. Tertiary stratigraphy and tectonic characters in the northern Tarim Basin. Science Press, Beijing, 97 pp.
Thompson, M.D., Bowring, S.A., 2000. Age of the Squantum 'tillite', Boston basin, Massachusetts: U–Pb zircon constraints on terminal Neoproterozoic glaciation. American Journal of Science 300, 630–655.
Vorob'eva, N.G., Sergeev, V.N., Knoll, A.H., 2009. Neoproterozoic microfossils from the northeastern margin of the East European Platform. Journal of Paleontology 83, 161–196.
Wang, Y., Chen, J., 1983. The petrographic characteristics and the age of Hongtiegou tillites from Xiaogaolu Group in Qinghai Province. Precambrian Geology 1, 145–162.
Wang, Y., Lu, S., Gao, Z., Lin, W., Ma, G., 1981. Sinian tillites of China. In: Hambrey, M.J., Harland, W.B. (Eds.), Pre-Pleistocene Glacial Record, IGCP 38. Cambridge University Press, Cambridge, pp. 386–401.
Wang, Y., Zhuang, Q., Shi, C., Liu, J., Zheng, L., 1980. Quanji Group along the northern border of Chaidamu Basin. In: Tianjin Institute of Geology and Mineral Resources (Ed.), Research on Precambrian Geology Sinian Suberathem in China, Tianjin, pp. 214–230.
Wang, J., Jiang, G., Xiao, S., Li, Q., Wei, Q., 2008. Carbon isotope evidence for widespread methane seeps in the ca635 Ma Doushantuo cap carbonate in South China. Geology 36, 347–350.
Xiao, S., et al., 2004. The Neoproterozoic Quruqtagh Group in eastern Chinese Tianshan: evidence for a post-Marinoan glaciation. Precambrian Research 130, 1–26.
Xing, Y., Ding, Q., Luo, H., He, T., Wang, Y., 1984. The Sinian–Cambrian boundary of China. Bulletin of the Institute of Geology. Chinese Academy of Geological Sciences, 1–262.
Xu, B., et al., 2009. SHRIMP zircon U–Pb age constraints on Neoproterozoic Quruqtagh diamictites in NW China. Precambrian Research 168, 247–258.
Yang, S., Zheng, Z., 1985. The Sinian trace fossils from Zhengmuguan Formation of Helanshan Mountain, Ningxia. Earth Science – Journal of Wuhan College of Geology 10, 9–18.
Zhao, X., Zhang, L., Zou, X., Wang, S., Hu, Y., 1980. Sinian tillites in Northwest China and their stratigraphic significance. In: Tianjin Institute of Geology Mineral Resources (Ed.), Research on Precambrian Geology Sinian Suberathem in China. Tianjin Science and Technology Press, Tianjin, pp. 164–185.
Zhou, C., Tucker, R., Xiao, S., Peng, Z., Yuan, X., Chen, Z., 2004. New constraints on the ages of Neoproterozoic glaciations in South China. Geology 32, 437–440.
Zhou, C., Xiao, S., 2007. Ediacaran $\delta^{13}C$ chemostratigraphy of South China. Chemical Geology 237, 107–126.
Zhu, X., 1957a. The major geological questions of the Chaidam Basin, part 1. Knowledge of Geology 6, 1–5.
Zhu, X., 1957b. The major geological questions of the Chaidam Basin, part 2. Knowledge of Geology 7, 9–14.